

## THERMAL AND VISUALISATION STUDY OF THE HFE7100 REFRIGERANT CONDENSATION PROCESS

Tadeusz BOHDAL<sup>✉</sup>, Małgorzata SIKORA<sup>✉</sup>, Karolina FORMELA<sup>✉</sup>

\* Faculty of Mechanical Engineering, Department of Energy Engineering, Koszalin University of Technology,  
 ul. Raclawicka 15-17, 75-620 Koszalin, Poland

[tadeusz.bohdal@tu.koszalin.pl](mailto:tadeusz.bohdal@tu.koszalin.pl), [malgorzata.sikora@tu.koszalin.pl](mailto:malgorzata.sikora@tu.koszalin.pl), [karolina.formela@s.tu.koszalin.pl](mailto:karolina.formela@s.tu.koszalin.pl)

received 27 February 2023, revised 5 June 2023, accepted 27 June 2023

**Abstract:** Technological advances are contributing to the search for highly efficient energy designs, and increasing interest in compact heat exchangers. Indeed, small channel diameters determine large heat transfer coefficients and condition a significant heat transfer area about the overall volume of the heat exchanger, as well as a smaller amount of refrigerant flowing in the system. Nevertheless, the operating stability and energy efficiency of compact heat exchangers are influenced by two-phase flow structures, which depend on thermal flow parameters. Knowledge of the structures formed during the condensation process is therefore essential for optimising the operation of refrigeration and air-conditioning equipment. This article presents the results from experimental studies of the HFE7100 refrigerant, from the hydrofluorocarbon group, condensation process in mini-channels with hydraulic diameters  $d_h = 2.0$  mm, 1.2 mm, 0.8 mm and 0.5 mm. Thermal flow characteristics were determined, and the forming structures of two-phase flow were recorded. The results of visualisation were subjected to morphological image analysis, based on a special algorithm written in MATLAB software. The algorithm makes it possible to determine the void fraction, which is necessary for calculating the vapour quality, as well as the area of vapour bubbles and their number, directionality and length along the x- and y-axes.

**Key words:** condensation, mini-channels, flow structures, HFE7100

### 1. INTRODUCTION

The condensation process is one of the frequently used phase transformations in heat pumps, refrigeration systems, air-conditioning systems, thermal power plants and heat recovery systems. The performance of these devices is significantly affected by the physical and chemical parameters of refrigerants [1]. The mutual configurations of the gas and liquid phases in radial and axial directions that form during the condensation process also affect the stability and efficiency of thermal machines [2]. However, their formation is interdependent on momentum and energy exchange mechanisms, which are directly shaped by changes in the conditions of the condensation process. Accordingly, thermal flow effects depend on flow structures. It should be noted that the diameter of the channel significantly affects the resulting flow structures of two-phase condensation, which are subject to changes in the length and cross-section of the channel [3, 4]. These changes are related to the type and nature of the flow, as well as the cross-section shape and spatial orientation of the channel. In addition, the formation of two-phase flow structures during condensation is affected by mechanisms of reciprocal relationships of internal forces that are formed in the area of the interfacial surface [5, 6]. It is worth noting that some structures intensify heat transfer, while others inhibit it. In terms of horizontal axis mini-channels, four main groups of structures can be distinguished, i.e. intermittent, dispersed, stratified and annular. Intermittent structures include slug and plug substructures. In the group of dispersed structures, which occur in the form of bubbles, droplets or particles suspended in the continuous phase, the

bubble and mist substructures are distinguished. Stratified structures include wave substructures. There are also transitional structures, such as the annular-wave flow. The most commonly observed structure in mini-channels is the annular flow. In micro-channels, a common structure is bubbly flow; dispersed, stratified and intermittent structures are observed much less frequently [7, 8]. The characteristics of the basic structures are described below (Fig. 1).

1. Mist flow—a structure in which the heat transfer process occurs with the highest intensity, while the pressure drops are the highest. With the increase in inertia forces, liquid droplets are entrained from the condensate film; hence, the liquid film disappears, and gas, in which there are fine liquid droplets, flows through the entire cross-section of the channel.
2. Bubble flow—a phase structure in which gas bubbles occupy a small part of the cross-section of the channel flow in the liquid phase.
3. Wave flow—liquid and gas flow through the channel co-currently, separated by strong gravitational force. Higher velocities of the gas phase determine the formation of disturbances at the boundary layer, resulting in the formation of waves on its surface. This contributes to an increase in the intensity of heat transfer.
4. Plug flow—gas bubbles of size comparable to the dimension of the channel diameter moving mainly in the upper part of the cross-section of the channel.
5. Slug flow—as a result of an increasing flow rate, shear stresses contribute to an increase in the range of waves responsible for the formation of gas bubbles according to the direction of

flow in the channel. As a result, large gas bubbles and some amount of liquid phase with small bubbles suspended alternately flow through the channel [9–11].

To recognize the conditions for the formation of two-phase condensation flow structures, it is necessary to conduct visualization studies [12]. The recorded image of the refrigerant flow, together with the thermal flow tests conducted, forms the basis for the development of maps of two-phase flow. These maps graphically depict the transition boundaries of the flow structures based on the characteristic parameters of phase transformation. They are usually two-dimensional drawings described by two quantities characteristic of the phenomenon [11].

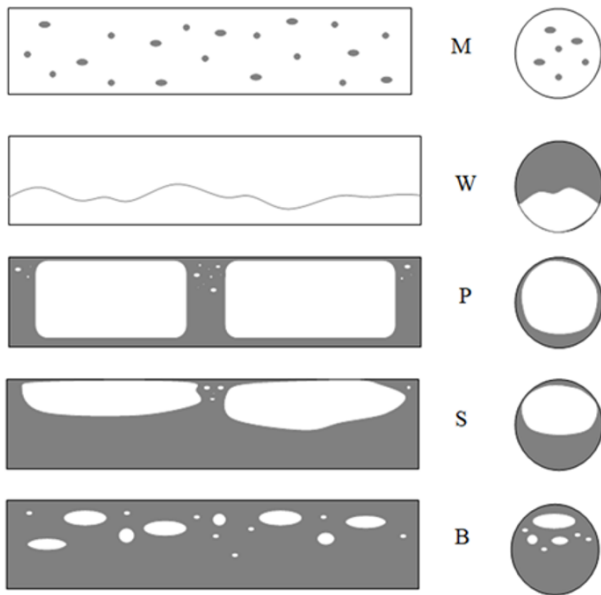


Fig. 1. Schematic view of described two-phase flow structures: M – mist flow, W – wave flow, S – slug flow, P – plug flow, B – bubbly flow

In nonadiabatic flows, the transition boundaries of structures are most often described by the vapour quality  $x$  and mass flux density  $G$ . These quantities, in addition to the flow parameters, also make it possible to consider parameters that describe heat transfer. Flow maps are important due to the increased interest in compact heat exchangers in air-conditioning and refrigeration solutions. Therefore, it is important to develop visualisation studies during the condensation process in mini-channels, which, due to the difficulty in the implementation of the condensation transformation itself, as well as in the measurement of its parameters, is much less frequently described compared to boiling or adiabatic two-phase processes [13].

Coleman and Garimella (1999, 2003) [7, 14] conducted an extensive study of two-phase condensation transformation during the flow of the R134a refrigerant in nine air-cooled mini-channels with circular, square and rectangular cross-sections in the range of hydraulic diameter  $dh = 1\text{--}4.91$  mm and mass flux density  $G = 50\text{--}150$  kg/(m<sup>2</sup>s). They conducted flow visualisation studies and observed intermittent, dispersed, annular and wave structures. In addition, they demonstrated the effect of vapour quality, flow rate and channel diameter dimension on the flow structures formed. They also showed the effects of gravity, inertia and interfacial interactions on the formed structures.

Sikora (2015) [15] carried out visualisation studies during the condensation process of the HFE7100 refrigerant in a mini-

channel with a hydraulic diameter of  $dh = 2.0$  mm in the mass flux density range below 200 kg/(m<sup>2</sup>s). Wave, plug, bubble and annular-wave structures were observed in the flow. This study reported that systematic studies of the condensation process of various low-pressure refrigerants may make it possible in the future to create a general structure map for refrigerants.

Al-Zaidi et al. (2018) [16] conducted a study of flow structures during the two-phase condensation flow of the HFE7100 refrigerant in a multiport, which was made in rectangular mini-channels with a hydraulic diameter of  $dh = 0.57$  mm in the mass flux density range  $G = 48\text{--}126$  kg/(m<sup>2</sup>s). They observed that at high mass flux densities, a ring structure was most often formed in the flow, while at lower values, a slug and bubble structure was observed.

Xiao and Hrnjak (2019) [17] presented the condensation results of the following refrigerants: R134a, R1234ze, R32, R245fa and R1233zd. These tests were performed in channels with a hydraulic diameter  $dh = 1.4\text{--}6.0$  mm. They described the exact conditions under which transitions between structures occur. According to this, in the annular flow, the influence of surface tension and shear forces prevails over gravity. The increase in the condensate film thickness affects the increase in the gravitational force impact. When its value exceeds the force of surface tension and shear stress, a stratified structure is formed in the flow. The formation of Kelvin–Helmholtz instability determines the transition between stratified and wave structures. Wave heights depend on the velocity difference of both, liquid and gas phases. At wave heights close to the inner diameter of the channel, the transition to an intermittent structure occurs. Indeed, low values of mass flux density determine low wave heights; hence, the discontinuous structure is not formed although there is an increase in the condensate film thickness.

Sikora (2020) [11] carried out visualisation studies of HFE7100, HFE7000 and Novec649 refrigerants under condensation conditions in mini-channels in the range of hydraulic diameter  $dh = 0.5\text{--}2.0$  mm, which were subjected to image analysis. As a result, the geometric dimensions of the structures, the vapour quality, the void fraction and the velocities of various phases were determined. The author analysed the results of modelling the heat transfer process and flow resistance; hence, it was shown that there are correlations between the flow resistance and the heat transfer coefficient with the type of two-phase flow structures. This paper mapped the flow structures considering the three factors studied and presented the conditions under which the transitions between the structures occur based on the magnitude of mass flux density and the void fraction.

## 2. RESEARCH STAND

Fig. 2 schematically illustrates the research stand for conducting thermal flow and visualisation tests during the condensation process of the HFE7100 refrigerant. From the analysis of this scheme, it can be observed that liquid refrigerant flows through the pump, and is successively pumped to the evaporator. An Endress + Hauser Coriolis mass flow meter 34XIP67 (accuracy class 0.5) is placed on the inlet to the evaporator. Then, using an electric heater system, heat flux is supplied to the refrigerant until it evaporates. The vapour of the refrigerant, at a constant temperature that is maintained by a thermostat, reaches the heat exchanger. This heat exchanger takes away the heat of vapour superheating to regulate the inlet vapour quality of the refrigerant. The next element is the measuring part of the research stand,

which includes a stainless steel mini-channel placed in the water channel. The refrigerant also flows through a glass mini-channel, where its flow is recorded with an Olympus i-speed 3 (CMOS) time-lapse camera (with a maximum recording speed of 10,000 fps and a maximum resolution of 1280 × 1024 pixels). The measuring section of the stand includes K-type thermocouples (with a thermocouple diameter of 0.1 mm), which are distributed along the length of the mini-channels and the water channel. A piezoresistive pressure sensor (with a measuring range of 0–40 MPa and a class of 0.5) and differential pressure transducer (Endress + Hauser Deltabar SPMP, with a measuring range of 0–1.5 MPa and a class of 0.075) are also mounted. After leaving the measuring section, the refrigerant flows into a water-cooled heat exchanger, which is responsible for its subcooling. Then, the refrigerant is directed to the liquid refrigerant tank. As a result, a series

of phase transformations begins again.

The research stand was subjected to tests to evaluate the correctness of its operation and zeroing of the measuring sensors. The test results are shown in Fig. 3. Testing of the stand consisted of passing only the liquid of the refrigerant through the measuring section and comparing the frictional coefficient of flow resistance with the results of theoretical calculations under the same conditions. For this purpose, the Blasius equation (Eq. [1]) and Hagen–Poiseuille equation (Eq. [2]) were used.

$$\lambda = 0.3164/Re^{0.25} \tag{1}$$

$$\lambda = 64/Re \tag{2}$$

As can be seen, the discrepancy between theoretical and experimental results is about ±20%.

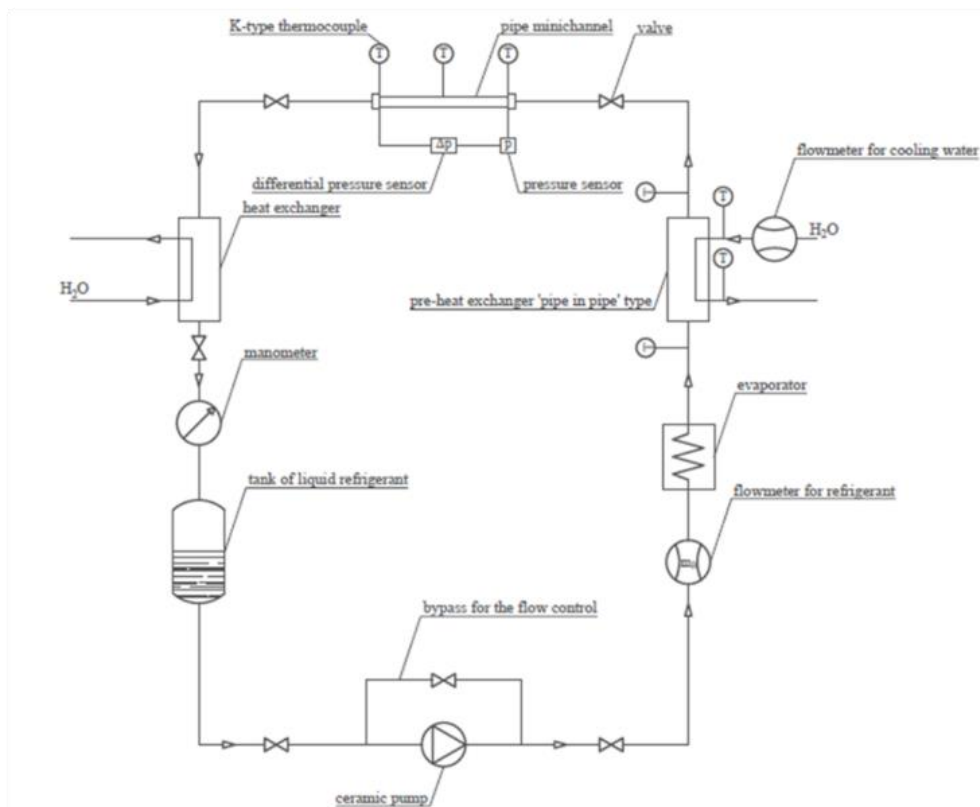


Fig. 2. Scheme of the test stand

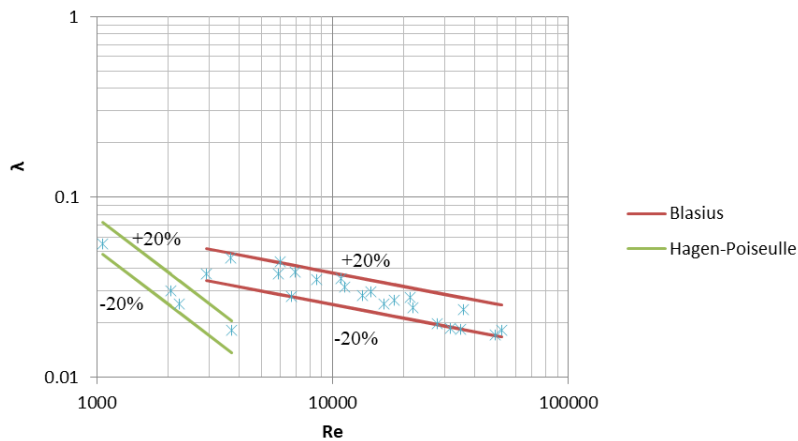


Fig. 3. Comparison of experimental and theoretical frictional coefficient of flow resistance λ versus Reynolds number Re for the HFE7100 agent in tubular mini-channels with internal diameter  $d_h = 0.5–2.0$  mm

### 3. RESEARCH METHODS

Determination of thermal flow characteristics of the condensation process and visualisation studies of two-phase flow structures were carried out simultaneously, which is innovative since previous studies have first performed thermal and then visualisation studies, such as Bohdal et al. (2015) and Sikora and Bohdal (2020) [15, 18]. In the thermal tests, the following parameters were measured using control and measurement equipment: the temperature of the wall surface and cooling water, as well as the mass flow rate of the cooling water and the refrigerant. The overpressure of the refrigerant on the inlet and the pressure difference along the length of the mini-channel were also measured directly. Appropriate instrumentation of the heat exchanger made it possible to record temperature measurements of the refrigerant and the cooling water, which in turn made it possible to determine the vapour quality of the refrigerant on the mini-channel, according to the equation:

$$\dot{Q} = \dot{m}_R \cdot c_R \cdot (T_R - T_S) + \dot{m}_R \cdot r \cdot (1 - x), \quad (3)$$

where  $\dot{m}_R$  is mass flux density of refrigerant,  $c_R$  is the specific heat of the refrigerant,  $T_R$  is the temperature of the refrigerant and  $T_S$  is the saturation temperature under given conditions and  $r$  is the unit heat of the phase transformation of condensation.

In the thermal study, the local value of the vapour quality  $x_i$  along the mini-channel during condensation was calculated by using the following equation:

$$x_i = x_{i-1} - \frac{[\dot{m}_w \cdot c_w \cdot (T_{wi-1} - T_{wi})]}{\dot{m}_r \cdot r}, \quad (4)$$

where  $x_{i-1}$  is vapour quality from the previous section,  $\dot{m}_w$  is mass flux density of the cooling water,  $c_w$  is the specific heat of the water,  $T_{wi-1}$  is the channel wall temperature in the previous section and  $T_{wi}$  is the channel wall temperature in this section.

Both the vapour quality and the heat flux density were determined indirectly, the values of which at individual cross-sections of the mini-channel made it possible to determine the heat transfer coefficient during the equation:

$$\alpha_i = \frac{q_i}{\Delta T_i}, \quad (5)$$

where  $\Delta T_i$  is the difference between the saturation temperature of refrigerant  $T_S$  and the temperature of the channel wall in a given cross-section  $T_{ci}$  under the given conditions.

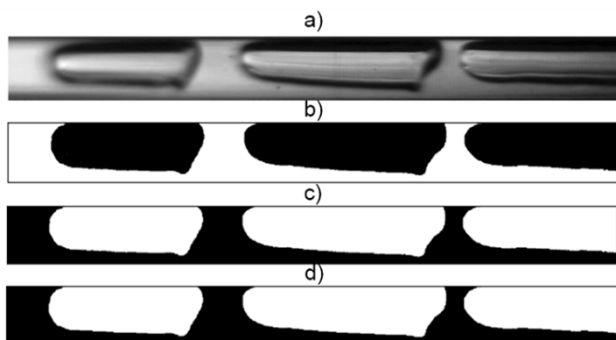


Fig. 4. Interpretation of image processing and analysis steps: a) image after cutting out the inside of the channel, b) binary image, c) image after inversion, d) image after noise removal

The computational method was also used to determine the mass flux density. To visualise the two-phase flow structures, a time-lapse camera was used to record images of the refrigerant flow. Frames were generated from the recorded image, from which the image of the inside of the mini-channel was sequentially cut out (Fig. 4a). In the next step, the phase separation line was closed. The image thus prepared was subject to morphological analysis by a special algorithm written in MATLAB R2019a. The algorithm performed binarisation (Fig. 4b), as a result of which black pixels occupied fields filled with the gas phase, while white pixels occupied those filled with the liquid phase. The next step was to perform inversion (Fig. 4c) and remove the “noise” (Fig. 4d). After this step, the gas phase was described by the white pixels, while the liquid phase was described by the black pixels. Based on the given image dimensions and the black and white pixels counted by the algorithm, the area occupied in the image by each phase was determined. The ratio of the area of the white pixels to the total area of the image is the void fraction  $\phi$ , and based on this, it is possible to determine the vapour quality  $x$  [19]:

$$x = \frac{\rho_v}{\left(\frac{\rho_l}{\phi} - \rho_l + \rho_v\right)}, \quad (6)$$

where  $\rho_l$  is the density of the liquid phase and  $\rho_v$  is the density of the vapour phase. A full description of the investigation methodology and accuracy of the measurement equipment is provided in the studies of Sikora et al. [18] and Sikora [19]. The heat transfer coefficient was determined with an accuracy of 10%, and the accuracy of pressure drop measurement was 8%. The vapour quality in visualisation studies was determined based on a two-dimensional image, and accordingly the accuracy of its determination is at the level of 12%.

### 4. PROPERTIES OF THE HFE7100 REFRIGERANT

A non-flammable, low-toxicity and thermally stable refrigerant from the hydrofluoroether group was used to perform thermal flow and visualisation studies. Selected physical properties of this odourless and almost colourless substance are shown in Table 1. The HFE7100 refrigerant is distinguished by its zero ozone depletion potential (ODP) and low global warming potential (GWP) parameter of 320. Its lifetime in the atmosphere is less than 5 years.

Tab. 1. Physical properties of the HFE7100 refrigerant for a temperature of 25°C and normal pressure

Chemical Formula	C <sub>4</sub> F <sub>9</sub> OCH <sub>3</sub>
Molar Mass [Kg/Kmol]	250
Boiling Point [°C]	61
Frizzing Point [°C]	-135
Liquid Density [Kg/M <sup>3</sup> ]	1510
Critical Pressure [Mpa]	2.23
Critical Temperature [°C]	195
Dielectric Constant	7.4
Latent Heat [Kj/Kg]	112
Specific Heat [J/(Kg·K)]	1170
Heat Conductivity [W/(M·K)]	0.0069
Vapour Pressure [Kpa]	26.9

Therefore, its environmental safety profile is excellent. In addition, its good dielectric properties mean that there is no risk of damage to electrical equipment during operation due to a leak or other failure. Most metals (aluminium, copper, brass, stainless steel) and hard polymers (polycarbonate, polypropylene, polyethylene, acrylic) offer a good compatibility as candidates for material to be used in the installation of the refrigeration circuit through

which the HFE7100 refrigerant flows. Based on the specified thermodynamic properties of the HFE7100 refrigerant, significant relationships were developed and used in the study. Fig. 5 illustrates some of them. A plot of the dependence of saturation temperature on saturation pressure was made. Characterisations of density, dynamic viscosity and specific heat of the liquid phase as a function of saturation temperature were also made.

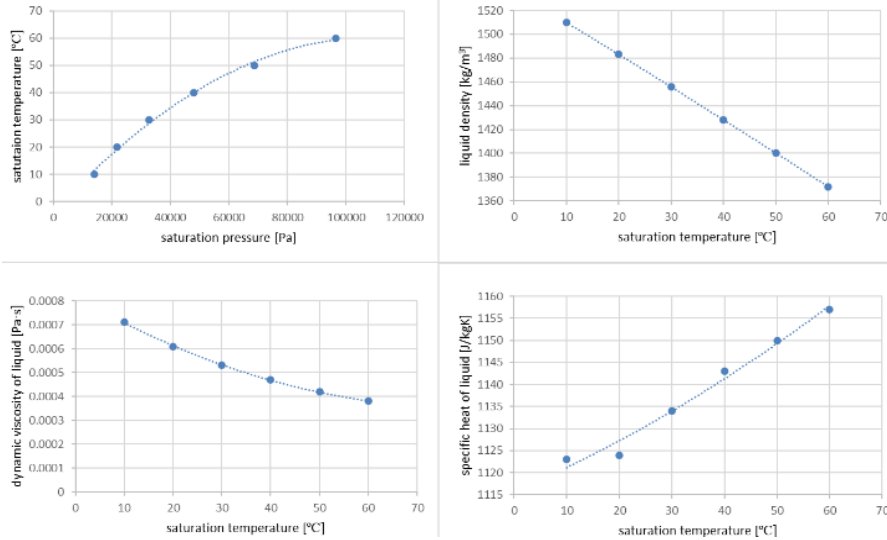


Fig. 5. Selected physicochemical relationships of the HFE7100 refrigerant

### 5. EXPERIMENTAL THERMAL FLOW CHARACTERISTICS

The basic thermal characteristic, which is the dependence of the heat transfer coefficient  $\alpha$  on the vapour quality  $x$ , is illustrated in Fig. 6. From its course in  $\alpha = f(x)$ , it can be observed that heat transfer intensifies as a result of the increase in the vapour quality and the density of the mass flow. One reason for this is the increase in turbulence due to higher refrigerant flow velocity, which results in more efficient heat transfer. In addition, increasing the

amount of the gas phase in the system also intensifies heat transfer, since gas has a higher thermal conductivity coefficient than liquids, and the condensate layer is similar to an insulator. From an analysis of the graphical summaries in Fig. 6, it can also be observed that a decrease in the dimension of the hydraulic diameter determines the increase in the value of the heat transfer coefficient. Indeed, increasing the energy efficiency of heat transfer has a beneficial effect on the two-phase transformation of condensation.

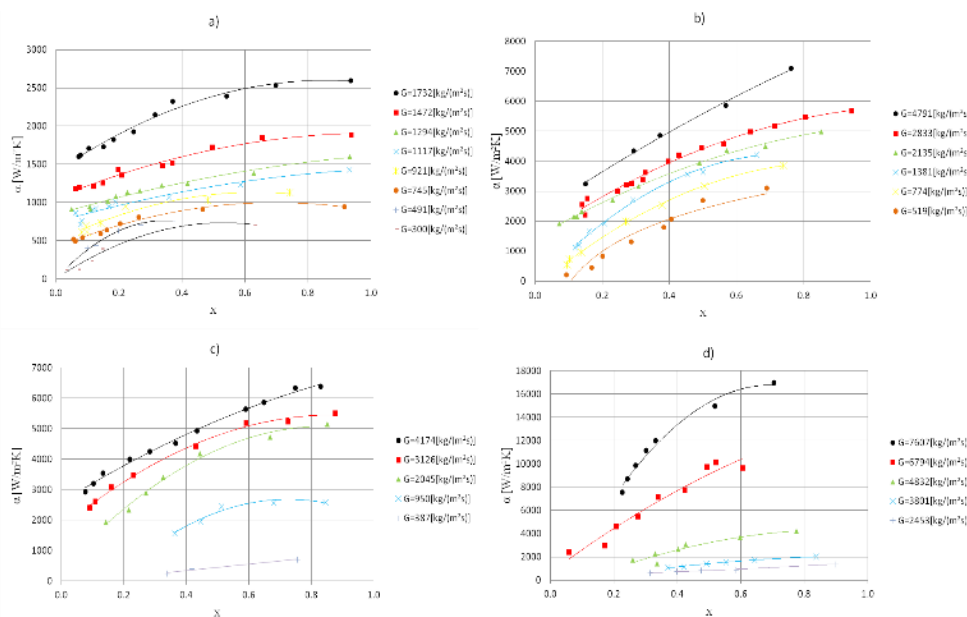


Fig. 6. Dependence of the heat transfer coefficient  $\alpha$  as a function of the vapor quality  $x$  for different mass flux densities  $G$  during the condensation process of the HFE7100 agent in a mini-channel with a diameter: a)  $d_h = 2.0$  mm, b)  $d_h = 1.2$  mm, c)  $d_h = 0.8$  mm, d)  $d_h = 0.5$  mm

Fig. 7 illustrates the dependence of flow resistance  $\Delta p/L$  as a function of vapour quality  $x$  for different values of mass flux density  $G$ . From the analysis of the characteristics presented in the graphical form, it is noticeable that the flow resistance increases with an increase of the vapour quality. Undoubtedly, the increas-

ing flow velocity of the refrigerant determines the increased pressure drop along the length of the mini-channel. The hydraulic diameter of the channel also has a significant impact on flow resistance. A decrease in its dimension contributes to an increase in flow resistance.

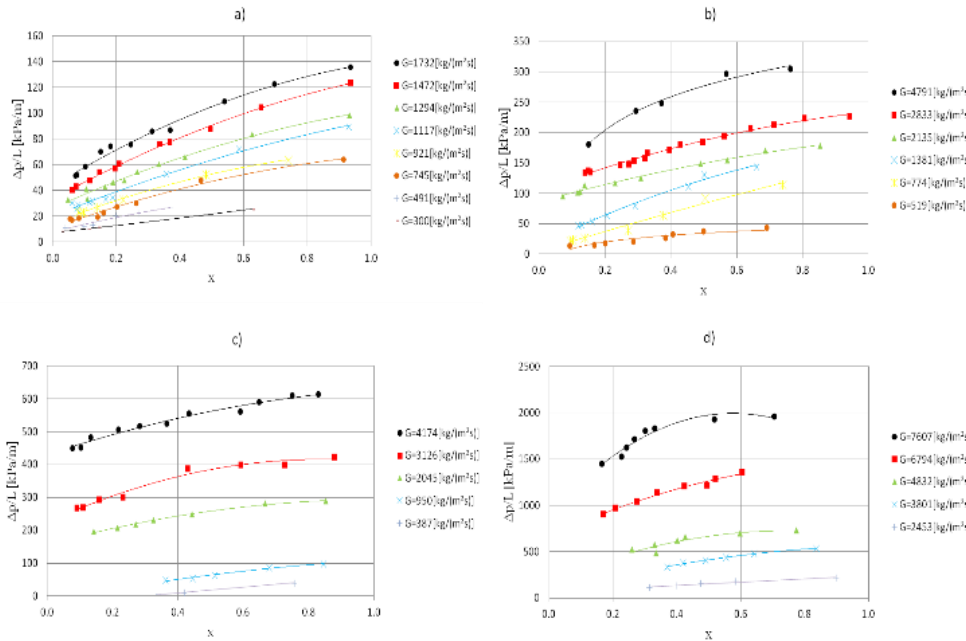


Fig. 7. Dependence of flow resistance  $\Delta p/L$  on the degree of dryness  $x$  for different mass flux densities  $G$  during the condensation process of the HFE7100 refrigerant in a mini-channel with diameter: a)  $d_h = 2.0$  mm, b)  $d_h = 1.2$  mm, c)  $d_h = 0.8$  mm, d)  $d_h = 0.5$  mm

## 6. RESULTS OF VISUALISATION STUDIES OF TWO-PHASE FLOW STRUCTURES

Example results of visualisation of two-phase condensation flow structures of the HFE7100 refrigerant in a mini-channel with a diameter of 2.0 mm are shown in Fig. 8. The following structures were observed: plug (Fig. 8a), bubble (Fig. 8b), annular-wave (Fig. 8c) and slug (Fig. 8d).

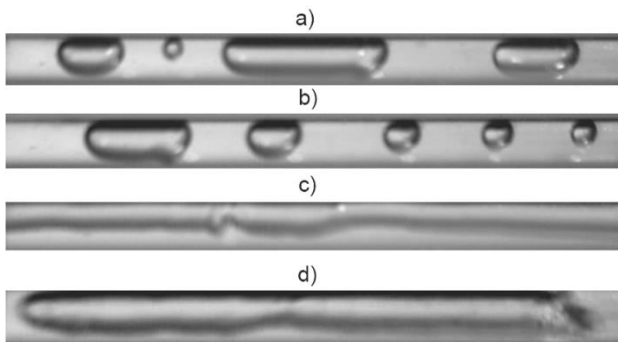


Fig. 8. Experimental results of visualization studies during the condensation process of the HFE7100 refrigerant in a mini-channel with a diameter of  $d_h = 2.0$  mm: (a) plug structure,  $G = 150$  kg/m<sup>2</sup>s,  $T_s = 67.4^\circ\text{C}$ ,  $\varphi = 0.36$ , (b) bubble structure  $G = 300$  kg/m<sup>2</sup>s,  $T_s = 67.1^\circ\text{C}$ ,  $\varphi = 0.23$ , (c) annular-wave structure  $G = 309$  kg/m<sup>2</sup>s,  $T_s = 67.6^\circ\text{C}$ ,  $\varphi = 0.56$ , (d) slug structure  $G = 504$  kg/m<sup>2</sup>s,  $T_s = 70.9^\circ\text{C}$ ,  $\varphi = 0.63$

Fig. 9 shows images of the structures that were observed during the testing of the condensation process of the HFE7100 refrigerant in a mini-channel with a diameter of 1.2 mm. In this case, bubble (Fig. 9a), plug (Fig. 9b), annular (Fig. 9c) and annular-wave (Fig. 9d) structures were observed. Example results of two-phase flow structures visualisation during condensation of the HFE7100 refrigerant in a mini-channel with a diameter of 0.8 mm are shown in Fig. 10. The following structures were observed: annular-wave (Fig. 10a), bubble (Fig. 10b), slug (Fig. 10c) and annular (Fig. 10d).

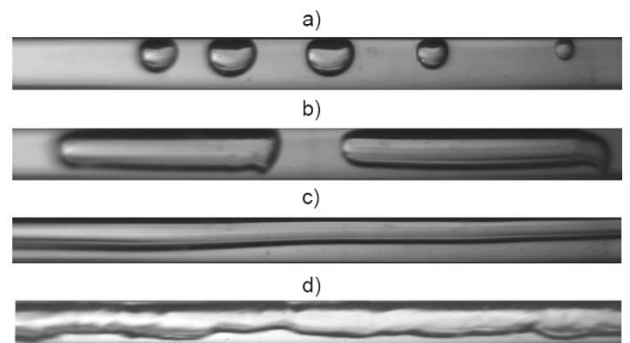
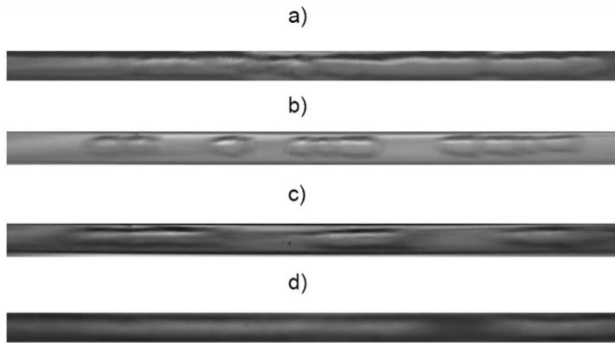
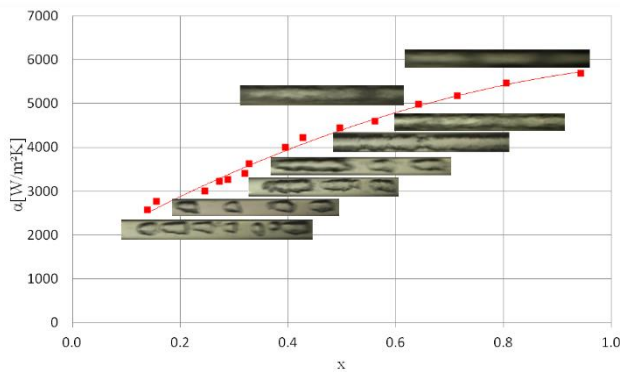


Fig. 9. Experimental results of visualization studies during the condensation process of the HFE7100 refrigerant in a mini-channel with a diameter of  $d_h = 1.2$  mm: (a) bubble structure  $G = 270$  kg/m<sup>2</sup>s,  $T_s = 70.7^\circ\text{C}$ ,  $\varphi = 0.17$ , (b) plug structure  $G = 491$  kg/m<sup>2</sup>s,  $T_s = 70.8^\circ\text{C}$ ,  $\varphi = 0.63$ , (c) annular structure  $G = 786$  kg/m<sup>2</sup>s,  $T_s = 71.1^\circ\text{C}$ ,  $\varphi = 0.62$ , (d) annular-wave structure  $G = 2801$  kg/m<sup>2</sup>s,  $T_s = 74.6^\circ\text{C}$ ,  $\varphi = 0.54$



**Fig. 10.** Experimental results of visualization studies during the condensation process of the HFE7100 refrigerant in a mini-channel with a diameter of  $d_h = 0.8$  mm: (a) annular-wave structure  $G = 884$  kg/m<sup>2</sup>s,  $T_s = 70.6^\circ\text{C}$ ,  $\varphi = 0.70$ , (b) bubble structure  $G = 884$  kg/m<sup>2</sup>s,  $T_s = 70.7^\circ\text{C}$ ,  $\varphi = 0.38$ , (c) slug structure  $G = 2045$  kg/m<sup>2</sup>s,  $T_s = 68.5^\circ\text{C}$ ,  $\varphi = 0.37$ , (d) annular structure  $G = 4257$  kg/m<sup>2</sup>s,  $T_s = 82.7^\circ\text{C}$ ,  $\varphi = 0.79$



**Fig. 11.** Two-phase flow structures in a mini-channel with diameter  $d_h = 1.2$  mm for mass flux density  $G = 2833$  kg/m<sup>2</sup>s,  $T_s = 74\text{--}78^\circ\text{C}$  during condensation of the HFE7100 refrigerant

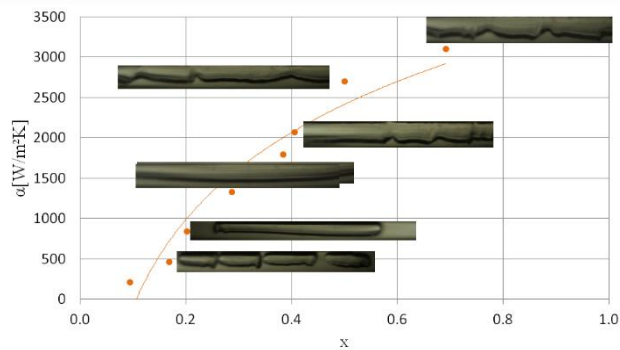


**Fig. 12.** Two-phase flow structures in a mini-channel with diameter  $d_h = 1.2$  mm for mass flux density  $G = 519$  kg/(m<sup>2</sup>s),  $T_s = 71\text{--}74^\circ\text{C}$  during condensation of the HFE7100 refrigerant

The type of structure formed is mainly influenced by flow parameters [20]. Among these are the mass flux density  $G$  and the liquid and vapour phase velocities, as well as the vapour quality  $x$  and the void fraction  $\varphi$ . As can be seen in Figs. 11 and 12, a change in the vapour quality  $x$  and mass flux density changes the flow structure that occurs, and these structures closely affect the intensity of heat transfer, i.e. an increase in the liquid phase

amount causes a decrease in the heat transfer coefficient. However, the shape of the phase separation surface is not insignificant. The more developed the phase separation surface, the higher the heat transfer coefficient resultantly obtained. The development of the phase separation surface is closely related to the flow velocity of the gas phase since a high value of it disturbs the interfacial surface.

## 7. CONCLUSIONS


Heat transfer and visualisation studies were carried out during the condensation process of a substance from the hydrofluoro-ether group, HFE7100, in horizontal mini-channels. Based on the obtained results, the dependence of the heat transfer coefficient and flow resistance as a function of the vapour quality was shown in a graphical form. An analysis of the effect of mass flux density and the dimension of the hydraulic diameter of the mini-channel on the energy efficiency of heat transfer and pressure drop along the length of the channel was carried out. The observed structures of two-phase flow during condensation of the HFE7100 refrigerant were presented. The following conclusions can be drawn from the experimental results obtained:

- A significant effect on the heat transfer coefficient  $\alpha$  is determined by the vapour quality  $x$  and the mass flux density  $G$ . Increasing the values of these parameters leads to an intensification of heat transfer. An increase in the heat transfer coefficient is also observed following a decrease in the dimension of the hydraulic diameter  $d_h$  of a single-pipe mini-channel.
- The value of flow resistance  $\Delta p/L$  is determined not only by the vapour quality  $x$  but also by the mass flux density  $G$ . Therefore, an increase in the vapour quality and mass flux density contributes to an increase in flow resistance. The dimension of the hydraulic diameter of the mini-channel also has a significant effect on flow resistance. Under the same conditions of the condensation process, an increase in the hydraulic diameter of the mini-channel is accompanied by a decrease in flow resistance.
- The type of structure formed is mainly influenced by the following flow parameters: mass flux density  $G$  and liquid and vapour phase velocity, as well as the vapour quality  $x$  and the void fraction  $\varphi$ .
- The thermal flow effects of two-phase condensation depend on the flow structure. On the other hand, some two-phase flow structures intensify heat transfer, whereas others limit the energy efficiency of heat transport (annular, annular-wave, slug and plug structures). Unfortunately, these structures with given higher heat transfer coefficients are given high pressure drops too.

## REFERENCES

1. Wang Z, Xu Z, Luo L, Xia X, Peng D, Li X. Experimental investigation of condensation pressure drop of zeotropic refrigerant/oil mixtures in plate heat exchanger. *International Journal of Refrigeration* 2023; 149: 192-203. <https://doi.org/10.1016/j.ijrefrig.2022.12.026>
2. Mikielewicz D, Andrzejczyk R, Jakubowska B, Mikielewicz J. Comparative study of heat transfer and pressure drop during flow boiling and flow condensation in minichannels. *Archives of Thermodynamics*. 2014; 35: 17–37. <https://doi.org/10.2478/aoter-2014-0019>

3. Jige D, Kikuchi S, Eda H, Inoue N, Koyama S. Two-phase flow characteristics of R32 in horizontal multiport minichannels. Flow visualization and development of flow regime map. *International Journal of Refrigeration* 2018; 95: 156–164. <https://doi.org/10.1016/j.ijrefrig.2018.09.005>
4. Doretti L, Zilio C, Mancin S, Cavallini A. Condensation flow patterns inside plain and microfin tubes: A review. *International Journal of Refrigeration*. 2013; 36: 567–587. <https://doi.org/10.1016/j.ijrefrig.2012.10.021>
5. Xiao J, Hrnjak P. A flow regime map for condensation in macro and micro tubes with non-equilibrium effects taken into account. *Int J Heat Mass Transf.* 2019; 130: 893–900. <https://doi.org/10.1016/j.ijheatmasstransfer.2018.10.081>
6. Soligo G, Roccon A., Soldati A. Mass-conservation-improved phase field methods for turbulent multiphase flow simulation. *Acta Mech.* 2019; 230: 683–696. <https://doi.org/10.1007/s00707-018-2304-2>
7. Coleman JW, Garimella S. Two-phase flow regimes in round, square and rectangular tubes during condensation of refrigerant R134a. *International Journal of Refrigeration* 2003; 26: 117–128. [https://doi.org/10.1016/S0140-7007\(02\)00013-0](https://doi.org/10.1016/S0140-7007(02)00013-0)
8. Fronk BM, Garimella S. In-tube condensation of zeotropic fluid mixtures: A review. *International Journal of Refrigeration* 2013; 36: 534–561. <https://doi.org/10.1016/j.ijrefrig.2012.11.030>
9. Garimella Srinivas FBM. Encyclopedia of two-phase heat transfer and flow I. Fundamentals and Methods II. Condensation heat transfer. World Scientific 2016
10. Dziubiński M, Prywer J. *Mechanika plynów dwufazowych*. Wydawnictwo Naukowo Techniczne, Warszawa 2009
11. Sikora M. Modelowanie struktur przepływu dwufazowego podczas skraplania w minikanalach 2020
12. Ligus G, Zając D, Masiukiewicz M, Anweiler S. A New Method of Selecting the Airlift Pump Optimum Efficiency at Low Submergence Ratios with the Use of Image Analysis. *Energies (Basel)* 2019; 12: 735. <https://doi.org/10.3390/en12040735>
13. El Hajal J, Thome JR, Cavallini A. Condensation in horizontal tubes, part 1: two-phase flow pattern map. *Int J Heat Mass Transf.* 2003; 46: 3349–3363. [https://doi.org/10.1016/S0017-9310\(03\)00139-X](https://doi.org/10.1016/S0017-9310(03)00139-X)
14. Coleman JW, Garimella S. Characterization of two-phase flow patterns in small diameter round and rectangular tubes. *Int J Heat Mass Transf.* 1999; 42: 2869–2881. [https://doi.org/10.1016/S0017-9310\(98\)00362-7](https://doi.org/10.1016/S0017-9310(98)00362-7)
15. Bohdal T, Sikora M, Widomska K, Radchenko AM. Investigation of flow structures during HFE-7100 refrigerant condensation. *Archives of Thermodynamics* 2016; 36: 25–34. <https://doi.org/10.1515/aoter-2015-0030>
16. Al-Zaidi AH, Mahmoud MM., Karayiannis TG. Condensation flow patterns and heat transfer in horizontal microchannels. *Exp Therm Fluid Sci.* 2018; 90:153–173. <https://doi.org/10.1016/j.expthermflusci.2017.09.009>
17. Xiao J, Hrnjak P. A flow regime map for condensation in macro and microtubes with non-equilibrium effects taken into account. *Int J Heat Mass Transf.* 2019. <https://doi.org/10.1016/j.ijheatmasstransfer.2018.10.081>
18. Sikora M, Bohdal T. Heat and flow investigation of NOVEC649 refrigerant condensation in pipe minichannels. *Energy* 2020. <https://doi.org/10.1016/j.energy.2020.118447>
19. Sikora M, Bohdal T, Formela K. Experimental Study of HFE 7000 Refrigerant Condensation in Horizontal Pipe Minichannels. *Materials*. 2021; 14: 6886. <https://doi.org/10.3390/ma14226886>
20. Chen Y, Gao H, Liu H, Chen D, Jiang J., Ma Z. Experimental investigation on condensation regimes and transition boundary during bubble condensation in narrow rectangular channel. *International Journal of Thermal Sciences* 2023; 188: 108212. <https://doi.org/10.1016/j.ijthermalsci.2023.108212>

Tadeusz Bohdal:  <https://orcid.org/0000-0002-0621-2894>

Małgorzata Sikora:  <https://orcid.org/0000-0001-8373-3573>

Karolina Formela:  <https://orcid.org/0000-0002-8289-652X>



This work is licensed under the Creative Commons BY-NC-ND 4.0 license.